

Microbial fuel cell-assisted biogenic synthesis of gold nanoparticles and its application to energy production and hydrogen peroxide detection

Md Rezaul Karim*, Thi Hiep Han^{*,**,***,†}, Sandesh Y. Sawant*, Jae-jin Shim*, Moon Yong Lee*,
Woo Kyoung Kim*, Jong Su Kim^{****}, and Moo Hwan Cho^{*,†}

*School of Chemical Engineering, Yeungnam University, Gyeongsan, Gyeongbuk 38541, Korea

**Laboratory of Theoretical and Computational Biophysics, Ton Duc Thang University, Ho Chi Minh City, Vietnam

***Faculty of Applied Sciences, Ton Duc Thang University, Ho Chi Minh City, Vietnam

****Department of Physics, Yeungnam University, Gyeongsan, Gyeongbuk 38541, Korea

(Received 12 November 2019 • Revised 29 February 2020 • Accepted 13 March 2020)

Abstract—This paper reports the simultaneous synthesis of gold nanoparticles (AuNPs) with a spherical and stable structure using microbial fuel cell (MFC) biofilms. The green, facile, chemical stabilizers and capping-agent free AuNPs synthesis allow the binder-free in situ decoration of AuNPs on MFC anode electrode with the help of special interactions of biofilm. The MFC with AuNPs decorated carbon foam anode electrode produced 62.5% higher (46.37 Wm^{-3}) power density than that of the MFC equipped with plain carbon foam anode (control). The AuNPs facilitated the good adhesion of bacteria, amplified the conductivity, and reduced the internal resistance, resulting in improved overall MFC performance. In addition, the peroxide-mimicking activity was evaluated and the MFC-synthesized AuNPs exhibited significantly higher peroxidase mimicking activity than the chemically synthesized AuNPs, thereby, allowing the easy and rapid colorimetric detection of hydrogen peroxide with a detection limit of $20 \mu\text{M}$.

Keywords: Gold Nanoparticles, Hydrogen Peroxide Detection, Microbial Fuel Cell, Power Generation

INTRODUCTION

The use of fossil fuels has resulted in global warming and the production of huge amounts of waste materials. The large consumption of energy to treat industrial and domestic wastewater is a matter of concern. Approximately 4% of the total electricity produced in the USA is utilized in the entire process of water treatment [1]. Therefore, alternative energy sources, such as biological renewable energy, can save energy and make the process environmentally sustainable. A microbial fuel cell (MFC) is a bio-electrochemical device that can convert chemical energy to electrical energy by consuming organic substances through micro-organism activity. This process can become an advanced renewable energy technology because the microbial metabolism reduces the organic pollutants and produces electricity simultaneously. MFCs are a fascinating topic of research, because of the potential applications, such as wastewater treatment, energy production, synthesis of noble materials, desalination of seawater, and remote sensors [2-5].

Although MFCs are an attractive technology, the production of energy by MFCs is still too low compared to other types of fuel cells due to ohmic losses and higher internal resistance [6]. Therefore, systematic research is needed to overcome the barrier and explore its multiple applications. Anode material used in an MFC plays a vital role in power production. Therefore, modification of the anode by increasing the electrical conductivity and biofilm growth on its

surface is an attractive research topic [7]. Metal nanoparticles are considered excellent catalysts to modify electrode surface. Compared to other metal nanoparticles, gold nanoparticles (AuNPs) exhibit the highest stability, good biocompatibility, high surface to volume ratio, surface energy, and excellent conductivity. Accordingly, AuNPs are used extensively to enhance the anode performance of MFCs [8,9]. Guo et al. and Alatraktchi et al. reported the modification of anode by AuNPs and found a significant increase in the power output as compared to unmodified anode [9,10]. All of the methods used for AuNPs modification are expensive and multi-step utilizing chemical as a binder that blocks the active area of nanoparticles. Therefore, in this work, a simple simultaneous synthesis method of AuNPs in MFC and its in situ decoration on an electrode by biofilm was employed and the result was investigated by standard techniques.

AuNPs possess unique properties and have multiple applications, such as drug delivery, biolabeling, biosensing, medical diagnostics, and cancer radiotherapy [11,12]. Although AuNPs can be produced by a wide range of methods, research is still being conducted to allow easy production and obtain products suitable for sensitive applications. The chemical synthesis method uses high temperatures, pressures, and toxic chemicals as reductants, stabilizers, and capping agents [13]. Therefore, it is essential to develop a biogenic synthesis method for green chemistry and to avoid expensive hazardous chemicals. Generally, plants, algae, bacteria, and fungi are used as the reducing and stabilizing agents for green synthesis [14-17]. Each method provides different AuNPs with a range of properties in terms of particle size and surface charge. Metal-reducing bacteria *Shewanella oneidensis* MR-1 (*S. oneidensis*) can provide elec-

[†]To whom correspondence should be addressed.

E-mail: hanthihiep@tdtu.edu.vn, mhcho@ynu.ac.kr

Copyright by The Korean Institute of Chemical Engineers.

trons to synthesize AuNPs that are highly stable, hydrophilic, and homogeneously shaped [18]. *S. oneidensis* also generates excess electrons and protons during MFC operation to produce electricity [19]. In addition, *S. oneidensis* multilayer aggregation to the electrode produces biofilm and transfers electrons derived from organic substances. In this experiment, AuNPs were synthesized by an *S. oneidensis* biofilm on the anode electrode of an MFC without using any chemical capping and reducing agent. Moreover, the *S. oneidensis* biofilms contain a matrix of “sticky” extracellular polymeric substances (EPS) that can hold the AuNPs on its surface [20–22]. Therefore, an in situ coating of AuNPs on the anode with the help of sticky EPS can be achieved together with the AuNPs solution.

AuNPs can provide rapid and simple colorimetric detection of hydrogen peroxide (H_2O_2) by catalyzing the peroxidase substrate, 3,3',5,5'-tetramethylbenzidine (TMB) [23]. The accurate and rapid determination of H_2O_2 is an important exercise often encountered in pharmaceutical, clinical, food, environmental analysis, and industrial laboratories [24,25]. Although colorimetric detection by AuNPs is simple, the catalytic activities of AuNPs toward the peroxidase substrate are dependent on its surface properties [23]. In this study, the biogenic as-synthesized AuNPs were examined to determine the intrinsic peroxidase-mimicking activity, compared to chemically synthesized AuNPs.

This study focused on the green synthesis of AuNPs by MFCs along with their applications to the production of bioenergy and the colorimetric detection of H_2O_2 . To the best of the authors' knowledge, this is the first report of the simultaneous synthesis of AuNPs by an *S. oneidensis* biofilm in an MFC anode and the in situ AuNPs decoration of an anode for bioenergy production.

MATERIALS AND METHODS

1. Materials and Chemicals

Chloroauric acid ($H AuCl_4 \cdot 4H_2O$) was procured from Wako Pure Chemical Industries, Ltd., Japan. Hydrogen peroxide (H_2O_2), sodium hydroxide (NaOH), and hydrochloric acid (HCl) were purchased from Duksan Pure Chemical Co., South Korea. The peroxidase substrate, 3, 3', 5, 5'-tetramethylbenzidine (TMB), was supplied by Sigma-Aldrich, Inc., USA. All other chemicals were of analytical grade and used as received. Deionized (DI) water was obtained from a PURE ROUP 30 water purification system. Carbon paper coated with a Pt catalyst (0.5 mg cm^{-2}) was purchased from Fuel Cell Earth LLC, US.

2. Construction of MFC Reactor and Biofilm Development

Two sets of H-Type MFCs reactors were designed using 300 mL glass bottles (Corning Inc., NY, USA; 300 mL capacity) separated by a proton exchange membrane (Nafion®117), as described previously [26]. The membrane was clamped and fitted with rubber gaskets. A piece of Pt coated carbon paper ($2.5 \text{ cm} \times 4.5 \text{ cm}$) was used as the cathode and a three-dimensional nitrogen-doped carbon foam ($2 \text{ cm} \times 4 \text{ cm} \times 0.5 \text{ cm}$) as the anode. The latter was prepared using a procedure reported elsewhere [27]. Both electrodes were connected with a titanium wire to complete the electrical circuit. The cathode chamber was filled with 250 mL of phosphate-buffered saline (PBS) at pH 7 (NH_4Cl 0.31 g L^{-1} , KCl 0.13 g L^{-1} , $NaH_2PO_4 \cdot 2H_2O$ 3.32 g L^{-1} , $Na_2HPO_4 \cdot 12H_2O$ 10.36 g L^{-1}) and sparged

with air continuously at $150 \text{ cm}^3 \text{ min}^{-1}$ using an air pump. The MFC setup and anode media, Luria Broth (LB), were autoclaved for 30 and 16 min, respectively, to eliminate contamination.

S. oneidensis strain were taken from -80°C glycerol stock and streaked onto LB agar plates, grown overnight at 30°C . Single colony was inoculated in LB broth in 250 mL flask and incubated overnight at 37°C with 250 rpm. Finally, *S. oneidensis* culture was re-inoculated into the MFC anode chamber containing the LB medium at a ratio of 1 : 100. During the experiment, a resistance of $1,000 \Omega$ was provided to complete the circuit and the surrounding temperature was controlled to 30°C . After two weeks of MFC operation when the voltage became stable, the fully developed biofilm attached to the carbon foam was used to synthesize the AuNPs. Throughout the entire process, power generation was recorded using a multimeter. All experiments were conducted in triplicate.

3. MFC-assisted Synthesis of AuNPs

After inoculation in anode chamber, *S. oneidensis* was attached on the anode rough surface and colonized the open-porous scaffold of carbon foam to form the biofilm. After two weeks of MFC operation, stable voltage outputs were observed, indicating that the biofilm was fully developed on anode electrode [28]. At that time the anolyte was replaced with the gold precursor, a 1 mM $H AuCl_4 \cdot 4H_2O$ aqueous solution in 250 mL of DI water and kept under magnetic stirring. Subsequently, sodium acetate (0.2 g) was added to the solution as an electron donor with constant stirring. Within 9 h, the initial yellow color began to change to purple. The reaction mixture solution was stirred for a further 3 h to complete the reaction. The as-synthesized AuNPs solution was then collected for characterization.

Two controlled experiments were carried out to investigate the role of the biofilm and sodium acetate in the AuNPs synthesis process. In the first control, the MFC was assembled with a plain carbon foam anode and anolyte containing 1 mM $H AuCl_4 \cdot 4H_2O$ and 0.2 g sodium acetate aqueous solution. In the second control MFC, the biofilm developed on the carbon foam was used as the anode and anolyte containing only a 1 mM $H AuCl_4 \cdot 4H_2O$ precursor. No color change was observed in both experiments during 12 hours operation. This suggests that both the biofilm and sodium acetate are involved in the synthesis of AuNPs.

4. MFC Performance using an AuNPs@carbon foam Anode

After complete synthesis of AuNPs in the MFC, the anode electrode (AuNPs@carbon foam) was removed to assess its potential for power generation in a new MFC. To explore the role of AuNPs on the MFC performance, two sets of MFCs, one MFC with the AuNPs@carbon foam anode and another MFC with plain carbon foam anode (control), were set up simultaneously under the same conditions. Both anode compartments contained 250 mL LB medium inoculated with *S. oneidensis*. The cathode compartments were filled with PBS 50 mM, pH 7 and commercial platinum-coated carbon paper was used as the cathode.

5. Electricity Measurement

A digital multi-meter (Keysight 34972A, Keysight Technologies, Inc., USA) connected to a personal computer was used to record the DC voltage output during the experiment at 5 min intervals. After 14 days of continuous operation when the voltage had stabilized, polarization curves were scanned by changing the external

resistance from 100 to 6,000 Ω . The power ($P=IV$) output was calculated from the data obtained from a Keysight 34972A and normalized to the surface area of the anode.

6. Characterization of Biogenically Synthesized AuNPs

The surface plasmon resonance (SPR) of the AuNPs was measured by UV/Vis spectroscopy (Optizen 2120UV, Mecasys Co., Ltd, Korea). The zeta potential was measured to determine the surface charge by measuring the electrophoretic mobility using a Delta Nano zeta potential (Beckman Coulter, USA). The nanoparticles were examined by high-resolution transmission electron microscopy (HRTEM; Tecnai G2F20, FEI, USA) operating at an accelerating voltage of 200 kV equipped with an energy dispersive X-ray (EDX) analysis system. Selected area electron diffraction (SAED) images were recorded using the TEM instrument.

7. Characterization of AuNPs@carbon Foam

X-ray diffraction (XRD, PANalytical, X'pert-PRO MPD) was carried out using Cu $K\alpha$ radiation ($\lambda=0.15405$ nm). The standard compound JCPDS data file was used to compare the XRD data. Scanning electron microscopy (SEM S-4800, Hitachi Ltd, Japan) and EDX were used to further characterize the surface of the AuNPs@carbon foam and confirm the existence of AuNPs in the sample.

Cyclic voltammetry (CV) and electrochemical impedance spectroscopy (EIS) were carried out using a potentiostat (Versa STAT 3, Princeton Research, USA). A standard three electrode system with a platinum plate as the counter electrode, Ag/AgCl in saturated KCl as the reference electrode, and AuNPs@carbon foam or plain carbon foam as the working electrode was used for CV and EIS studies. Sterilized LB was used as the electrolyte and all experiments were conducted at room temperature.

A biocompatibility test was performed by counting the colony-forming units (CFU) on the electrodes to assess bacterial growth on the anode materials [29]. Briefly, after 14 days of MFC operation, a plain carbon foam and AuNPs@carbon foam were removed from the MFC and washed lightly to detach the loosely adhered

bacteria cells. A small portion of the electrode (1 cm \times 1 cm) was cut and sonicated for 5 min in 10 mL of sterile phosphate buffer. The bacterial suspension was then spread over the LB agar plates and incubated overnight at 37 $^{\circ}$ C. The CFU was calculated after counting the colonies on the agar plate. The experiment was conducted under sterile conditions in duplicate.

8. Morphological Characterization of Electrodes

The surface morphology of the AuNPs@carbon foam and plain carbon foam was examined by SEM. The analysis was conducted after 14 days of MFC operation using the procedure described elsewhere [30]. The anode-enriched biofilm was washed lightly with the buffer solution (phosphate buffer pH=7) to remove the loosely attached cells. The used anode was cut into small pieces, 0.4 cm \times 0.4 cm in size, and incubated overnight at 4 $^{\circ}$ C in a buffer containing a 2.5% glutaraldehyde and 2% formaldehyde solution. Subsequently, the samples were washed with 0.2 M sodium phosphate buffer and soaked in an osmium solution (1.5 mL of 0.2 M sodium phosphate buffer, 3 mL of 2% OsO₄ and 3 mL deionized water) for 90 min. The samples were dehydrated with a graded series of ethanol (50, 70, 80, 90, 95, and 100%) in chronological sequence at 30 min intervals. The specimens were then incubated in amyl acetate for 20 min and dried in a critical point dryer (HCP-2, Hitachi Ltd., Japan). The samples were then coated with platinum for 90 seconds by ion sputtering (E-1030, Hitachi Ltd., Japan) for SEM analysis.

9. Peroxidase-mimic Activity of Biogenic Synthesized AuNPs

The H₂O₂ colorimetric detection protocol is described elsewhere [31]. Briefly, 500 μ L of 5 mM TMB, 200 μ L of 6.58 nM AuNPs and 200 μ L of H₂O₂ at different concentrations (0.02 mM to 5 mM) were mixed with 730 μ L of 0.5 M acetate buffer (pH 4). The solution was incubated at room temperature for 5 min and the absorbance was measured by UV/Vis spectroscopy. The peroxidase-mimicking activity of biogenic-synthesized AuNPs (B-AuNPs) was compared with that of chemically synthesized AuNPs using the Turkevich method (C-AuNPs) [32]. The concentration of C-AuNPs was cal-

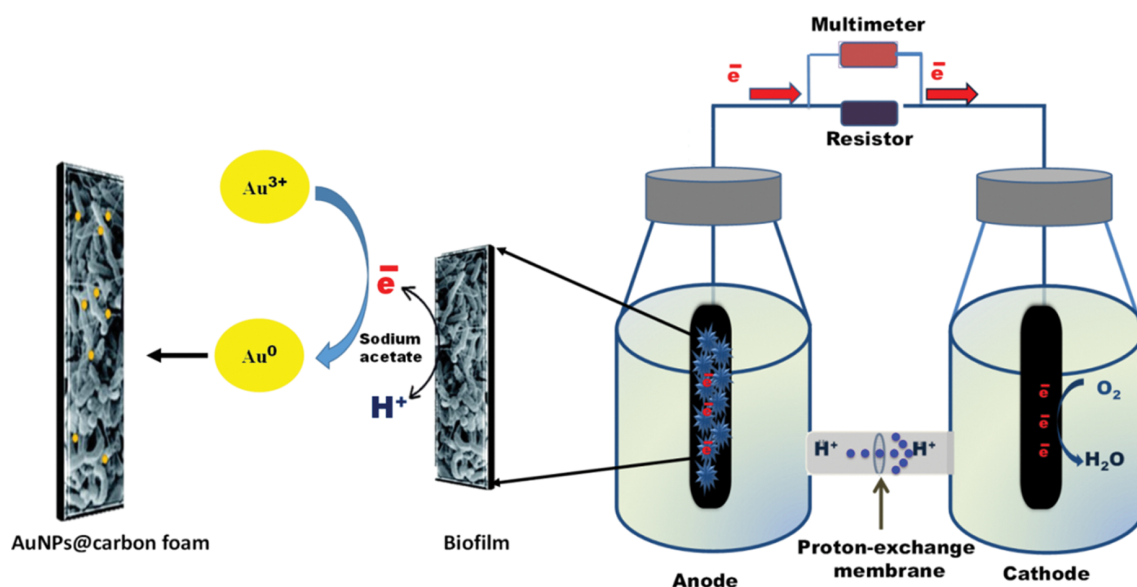


Fig. 1. Schematic model of the synthesis of AuNPs in a MFC anode chamber.

culated and presented in the supplementary information.

RESULTS AND DISCUSSION

1. Proposed Mechanism for the MFC-assisted Biogenic Synthesis of AuNPs

Simple one-step green synthesis occurred at the anode biofilm, which provided electrons from sodium acetate decomposition. Sodium acetate oxidized to produce electrons and was used as the organic electron donor [33]. The excess electrons reacted with chloroauric acid and reduced Au^{3+} ions to Au^0 , leading to AuNPs formation. The formation of AuNPs in the anode chamber was indicated by a yellow to purple color change within 12 h [16,34]. Fig. 1 presents a schematic model of the proposed AuNPs synthesis in the anode chamber of MFC. The proposed method provides a simple and one-step environmentally favorable approach that governs at room temperature without using toxic reducing agents.

The colloidal aqueous solution SPR was recorded by UV-vis spectroscopy and showed a gradual increase in the SPR peak centered at 540 nm (Fig. 2), indicating the formation of AuNPs [35]. The absorbance spectra of the as-synthesized AuNPs was tested every week and provided the same results, even after a one month reaction. This means that there was no ageing effect or Ostwald ripening of the nanoparticles. The nanoparticle suspension remained

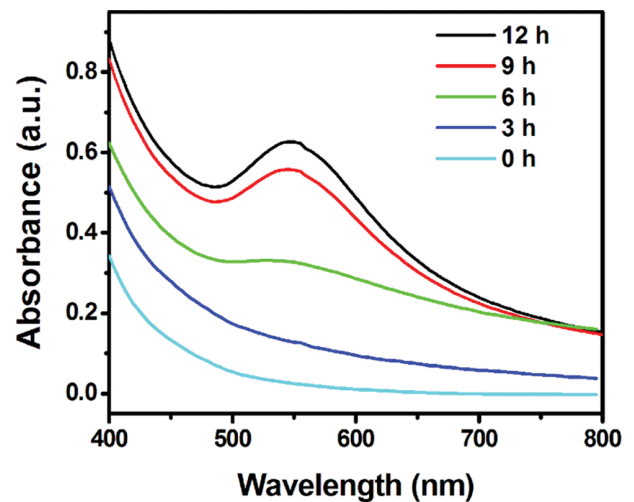


Fig. 2. UV-vis spectroscopy showing a peak at 540 nm indicating the formation of AuNPs.

stable without agglomeration for several months. This suggests that the as-synthesized AuNPs by the *S. oneidensis* biofilm in the anode chamber of the MFC are quite stable.

Zeta-potential analysis of the as-synthesized AuNPs showed that

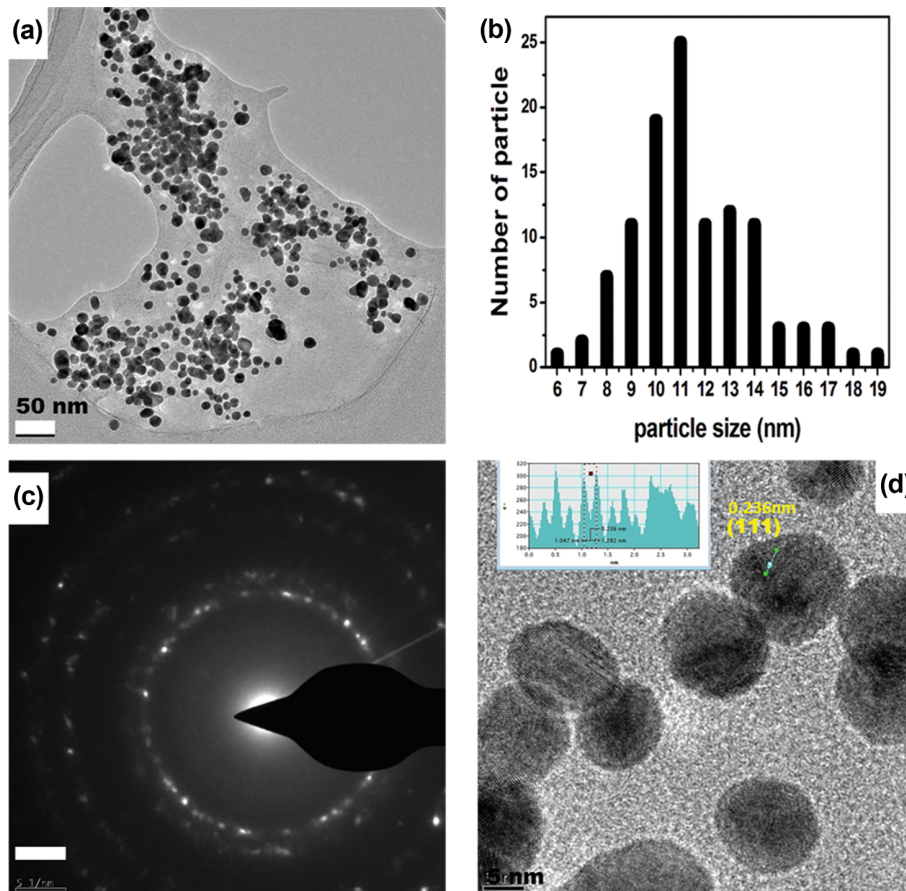


Fig. 3. (a) TEM image of AuNPs (b) particle size distribution of the as-synthesized AuNPs, (c) selected area electron diffraction (SAED), (d) HRTEM image with a d-spacing of 0.236 nm between the lattice planes.

the nanoparticles were negatively charged (-12.4 mV). The negatively charged AuNPs repel each other, which may prevent aggregation and promote dispersion over the anode surface.

TEM (Fig. 3(a)) showed that the spherical AuNPs were almost uniform and separated from each other. The mean size of the as-synthesized AuNPs particles was 12.5 ± 4.28 nm (Fig. 3(b)). SAED revealed bright circular rings, suggesting the as-synthesized AuNPs were highly crystalline (Fig. 3(c)). Fig. 3(d) presents an HR-TEM image at 5 nm resolution, illustrating lattice fringes on the spherical AuNPs. The calculated d-spacing of 0.236 nm is related to the (111) plane of the AuNPs (JCPDS card no: 04-0784, supported XRD information).

2. AuNPs@carbon Foam Characterization

XRD and EDX of AuNPs@carbon foam were conducted to confirm that the AuNPs had decorated the carbon foam successfully. XRD of the anode electrode with Cu $K\alpha$ radiation (Fig. 4) confirmed crystalline AuNPs formation where sharp XRD peaks were observed between 10 – $80^\circ 2\theta$. The prominent peaks were assigned to the (111), (200), (220), and (311) planes of face-centered cubic (fcc) gold, respectively (JCPDS powder diffraction file no 4-0784) and other two planes (002) and (100) related to graphitic carbon [36,37]. No other peaks were observed on the XRD pattern, indicating carbon foam had been decorated successfully with extremely pure AuNPs.

The EDX analysis of AuNPs revealed Au peaks, providing strong evidence of the presence of AuNPs on the carbon foam (Fig. 5). The percentage of AuNPs was estimated to be approximately 6.13%.

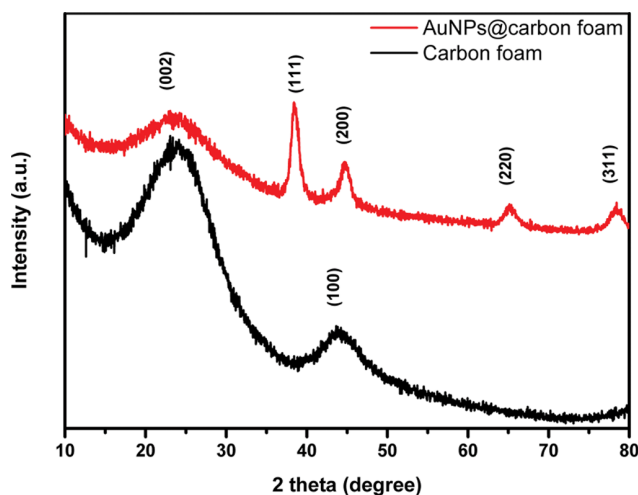


Fig. 4. XRD patterns of carbon foam and AuNP-decorated carbon foam.

The elemental mapping of AuNPs@carbon, presented in Fig. 5(d), revealed uniform distribution of Au over the carbon foam surface. The simultaneous synthesis and in situ decoration of AuNPs on the carbon foam anode were attributed to the strong electrostatic attraction of the nanoparticles towards the bacterial outer membrane [38]. Moreover, a collection of surface-attached microbial cells is called a biofilm, providing sorptive sponge capability to bind the AuNPs to its surface [39].

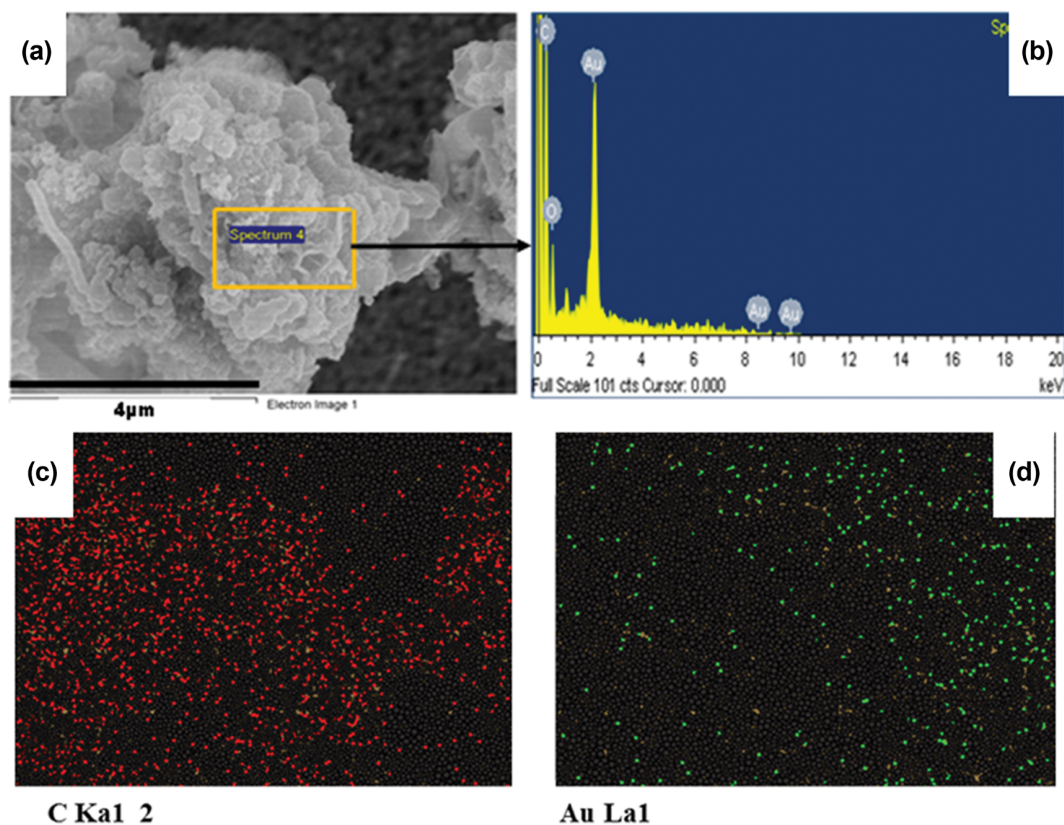


Fig. 5. Energy dispersive X-ray (EDX) analysis of the AuNPs@carbon foam anode (a)–(b), distribution of Au nanoparticles and carbon (c)–(d).

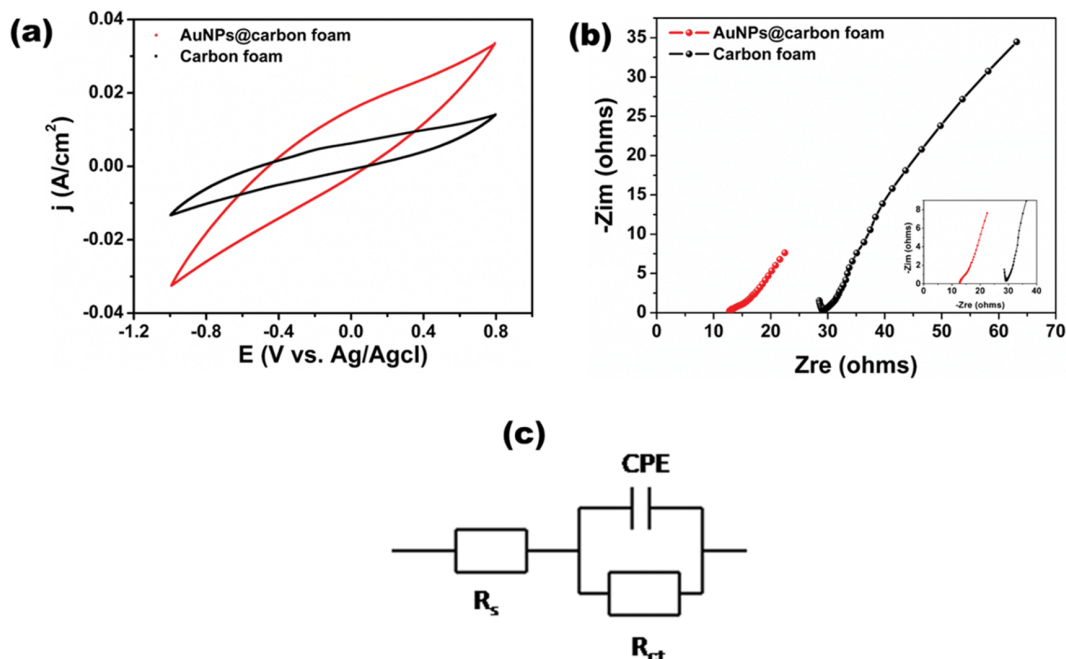


Fig. 6. (a) Cyclic voltammograms at a scan rate of 10 mVs^{-1} , (b) Nyquist plot of the AuNPs @carbon foam and plain carbon foam anode. (c) An equivalent circuit from the Nyquist plots.

3. Electrochemical Activity of AuNPs@carbon Foam

The electrochemical behavior of the AuNPs@carbon foam as an electrode material was examined by CV and EIS. CV defines the electrode characteristics, and EIS defines the solution conductivity at a current collector, conductivity between current collector active material, and active material electrolyte interphase. Fig. 6(a) presents the CV carried out at a scan rate of 10 mVs^{-1} within a potential window of -1.0 to 0.8 V . The CV curve of the AuNPs@carbon foam showed a larger area than the plain carbon foam, suggesting the modified carbon foam has higher charge storage capacity than its counterpart [40].

These results indicate the rapid current response to voltage reversal (small contact resistance) and reveal the higher capacitive behavior of the electrodes. Therefore, the CV curves show an ovoid shape, which could be attributed to the electrode-inherent resistance [41].

EIS of the AuNPs@carbon was performed to understand the charge process and transport properties of the AuNPs, as shown in Fig. 6(b). In general, the complex impedance plot is normally obtained as Z_{re} vs. Z_{im} , generated from the resistance and capacitance component of the electrochemical cell. The data is fitted using a fitting algorithm by a Randles-type equivalent circuit (supplementary information). The electrical equivalent circuits contain a solution resistance, a charge transfer resistance and a constant phase elements (CPE) [42]. The latter represents double-layer capacitance [43]. The EIS fitting data values are recorded in Table 1 and the experimental values obtained from the impedance data. In a Nyquist plot, the intercept on the Z_{re} axis represents the internal resistance (R_s) at the high frequency end, related to the ionic resistance of the electrodes, intrinsic resistance of the substrate and contact resistance between active material and current collector. The values of R_s of the AuNPs@carbon foam were lower than that of

Table 1. Fitting circuit values from equivalent circuit to analyze the Nyquist plots

Sample	R_s ($\Omega \text{ cm}^2$)	R_{ct} ($\Omega \text{ cm}^2$)	CPE ($\Omega^{-1} \text{ sn cm}^{-2}$)	n
Plain carbon foam	29.72	109.69	0.3514	0.73
AuNPs @carbon foam	17.08	66.58	0.3976	0.48

plain carbon foam. This significant decrease in R_s accelerated the electron transfer rate between the electrode and electrolyte. The interfacial charge (R_{ct}) is related to the semicircular diameter of the materials and small diameter suggest lower charge transfer resis-

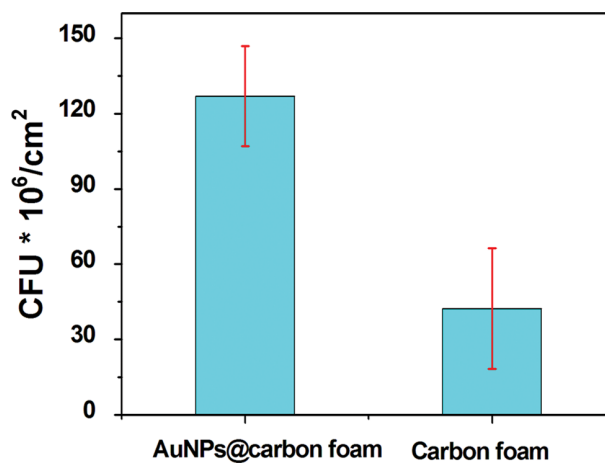


Fig. 7. Colony-forming unit (CFU) of *S. oneidensis* on AuNPs@carbon foam and plain carbon foam.

tance. The AuNPs@carbon foam exhibited lower charge transfer resistance indicating good conductivity resulting acceleration of electron transfer rate. The AuNPs decorated on the electrode increases the conductivity, providing a larger active area for the colonization of bacteria and therefore better electrochemical performance.

4. Biocompatibility and Surface Morphology Analysis

The biocompatibility of the plain carbon foam anode and AuNPs@carbon foam was examined by counting the *S. oneidensis* colony formation on these electrodes. Fig. 7 shows the difference in CFU on the AuNPs@carbon foam and plain carbon foam. The number of viable bacteria cells attached to the AuNPs@carbon foam was $127 \pm 20 \times 10^6$ CFU cm^{-2} , which was three times higher than that to the plain carbon foam ($42.3 \pm 24 \times 10^6$ CFU cm^{-2}). The higher CFU on AuNPs@carbon foam provides evidence that the carbon foam modified with AuNPs contained a larger number of bacteria cells than the plain carbon foam.

Fig. 8(a) and 8(d) present SEM images of the surface morphology of two different anodes after 14 days of MFC operation. The structured community of bacterial cells was much higher (Fig. 8(c) and (d)) on the AuNPs@carbon foam surface than on the plain carbon foam (Fig. 8(a) and (b)), which is in accordance with the biocompatibility result. *S. oneidensis* covered not only the entire surface but also the internal pores of the 3D carbon foam. The larger amount of bacterial attachment to the AuNPs@carbon foam leads to better MFC performance. The surface roughness of the electrodes is one of the important factors for bacteria adhesion. Emerson et al. and Wei et al. reported that AuNPs decoration on the anode enhances the surface roughness and subsequently pro-

vides good adhesion for bacterial colonization [7,44]. The good conductivity of AuNPs was also reported to accelerate electron transfer; hence, *S. oneidensis* can attach to the electrode and donate electrons easily, which is helpful for enhancing biofilm growth on the electrode surface [45]. Moreover, the increase in surface roughness might have kept the bacterial colony adhered and prevented the detachment of loosely attached bacteria.

5. MFC Performance during AuNPs Synthesis

After two weeks operation, when MFC-1 (plain carbon foam anode) produced a stable voltage and biofilm formation was fully developed, the anode media was replaced with the gold precursor (MFC-2). During 12 hours of AuNPs synthesis, 33.92 Wm^{-3} maximum power generation under this condition was also observed. Fig. S1 (see Supplemental Information) presents a graph showing that MFC-1 achieved the maximum voltage (0.37 V) at 109.5 hours operation, whereas MFC-2 produced the same value at 9.5 hours operation, which was 11.5 times shorter than that of the first stage of the MFC.

The shorter time could be due to the following reasons. (i) The gold precursor, chloroauric acid (pH 4), provided more protons in the solution, which may have passed through the proton exchange membrane, leading to a higher current as well as reduced internal resistance and higher proton flux. (ii) The acidic conditions provide a better environment to grow more bacterial cells. This may be one of the reasons for the improved MFC performance. Several studies have examined how acidity influences the performance of metal-reducing bacteria. Justin et al. reported that acidity increases the *S. oneidensis* cell concentration [46]. Gaboriaud et al. also showed

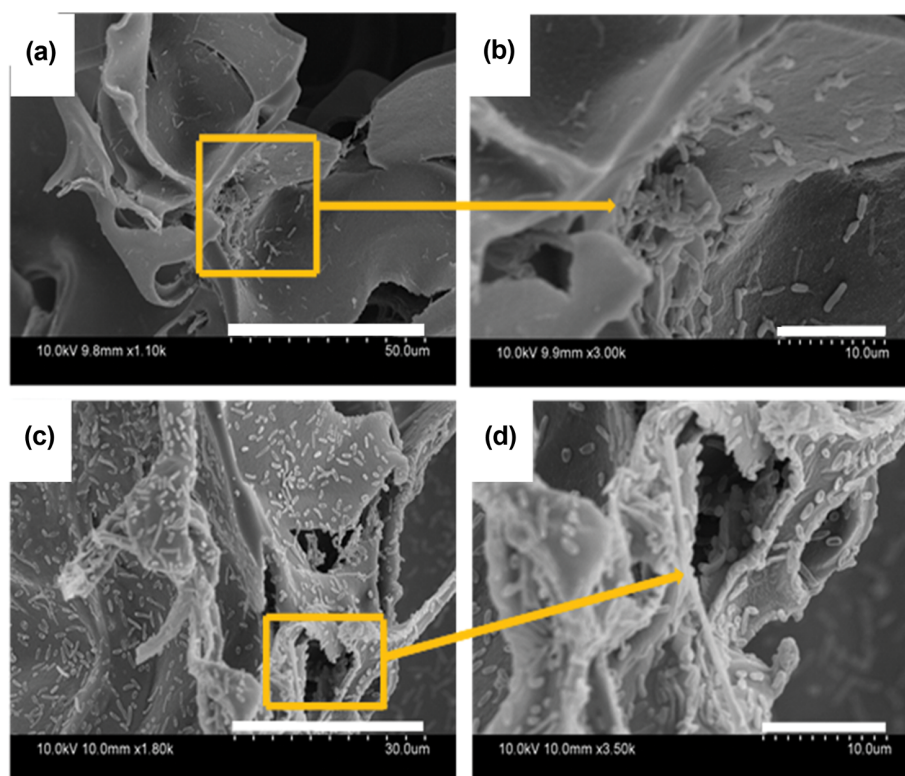


Fig. 8. *S. oneidensis* MR-1 attached to the surface of the carbon foam anode (a)-(b) and AuNPs@carbon foam anode (c)-(d) after running the MFCs for 14 days.

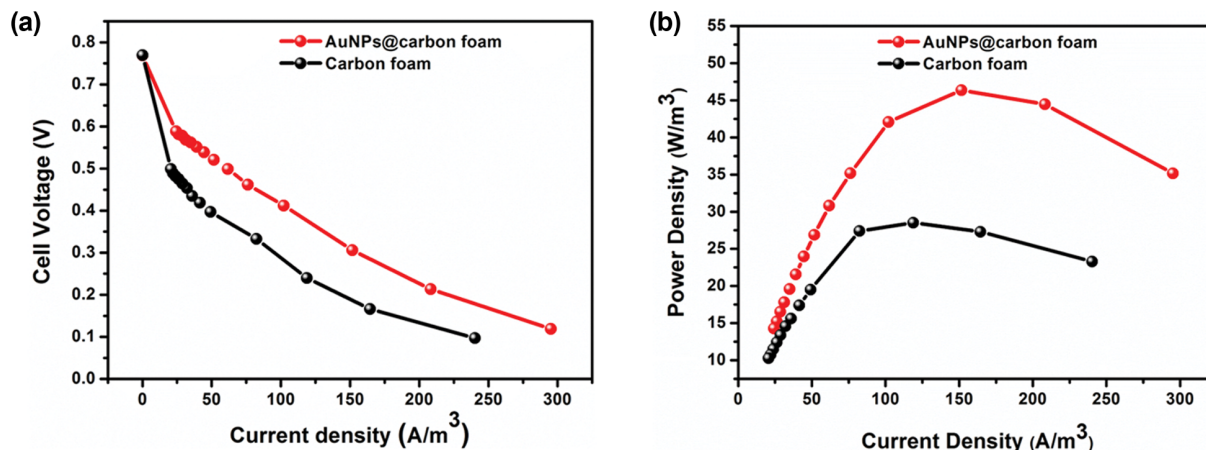


Fig. 9. (a) Polarization curve, (b) Power curve of MFCs with plain carbon foam and AuNPs @carbon foam anode.

that decreasing the pH from 10 to 4 affects the adhesion and physiology of *Shewanella* sp., which improves the rate of electron transfer during power production [47].

6. MFC Performance of the AuNPs@carbon Foam Anode

After in situ decoration of carbon foam as the anode by AuNPs (AuNPs@carbon foam) in the MFC-2, further AuNPs@carbon foam was applied in the new MFC to monitor its efficiency in the power generation application. Fig. 9 represents the polarization and power density *versus* the current density of the AuNPs@carbon foam and compares them with the plain carbon foam anode electrode. The MFC with the AuNPs@carbon foam anode generated a maximum power density of 47.37, which was approximately 1.6-times higher than that MFC using the plain carbon foam anode. This suggests that the AuNPs enhance the MFC performance. The open circuit voltage (OCV) of both electrodes was similar (0.77 V), indicating that they have similar activation resistance. The voltage of the carbon foam decreased rapidly compared to the modified carbon foam (Fig. 9(a)), showing the losses by mass transport and ohmic losses were higher in the case of the plain carbon foam [48]. The power

density peak method was used to determine the internal resistance and according to this method; the internal resistance is equal to the external resistance when the power density reached its peak [49]. During that time, the internal resistance of the AuNPs@carbon foam MFC was 500 Ω , whereas that of the control MFC was 1,000 Ω . The lower internal resistance of the modified electrode resulted in higher MFC performance.

7. Hydrogen Peroxide Detection

The MFC-assisted biogenic synthesized AuNPs (B-AuNPs) was used to catalyze the oxidation of the peroxidase substrate, 3, 3, 5, 5-tetramethylbenzidine (TMB), to detect H₂O₂. The detection principle is reported elsewhere [50]. Briefly, the negatively charged AuNPs electrostatically attract two amino groups present in TMB, showing strong affinity with TMB as a reaction substrate [7]. The AuNPs catalyze the oxidation of TMB in the presence of H₂O₂, resulting in the formation of a blue-charge transfer complex in a very short time and provides the maximum absorbance at 655 nm.

To compare the colorimetric detection with the as-synthesized B-AuNPs, chemically synthesized AuNPs (C-AuNPs) were pre-

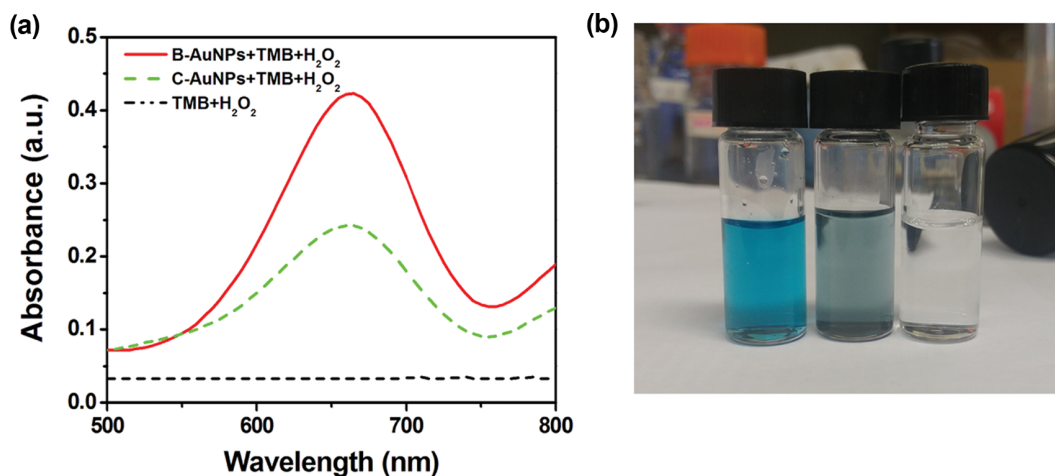


Fig. 10. UV-vis absorption spectra (a), as seen by a naked eye examination of the colorimetric detection of H₂O₂, (b) (left to right: as-synthesized biogenic AuNPs (B-AuNPs+TMB+H₂O₂), citrate-capped AuNPs (C-AuNPs+TMB+H₂O₂) and in the absence of catalyst (TMB+H₂O₂)).

pared using trisodium citrate salts as a reducing agent according to previously published protocols [51]. The blue color developed in the presence of B-AuNPs+TMB+H₂O₂ was darker and faster (5 minutes) than in the presence of C-AuNPs+TMB+H₂O₂ (10 minutes), while there was no color change in the absence of a catalyst in TMB+H₂O₂ solution (Fig. 10(b)). The UV spectra in Fig. 10(a) also showed that the absorbance of B-AuNPs+TMB+H₂O₂ was highest compared to the others. Therefore, the peroxidase-mimicking activity of B-AuNPs is higher than that of C-AuNPs.

The rapid and sharp H₂O₂ detection in the case of B-AuNPs catalyst compared to C-AuNPs can be attributed to the following factors. (i) The B-AuNPs were smaller (12 nm) than the C-AuNPs (17 nm) providing a larger surface-to-volume ratio. The higher surface area allowed more contact with the substrate, resulting in higher performance [10]. (ii) The citrate cap covered the active sites of the nanoparticles, which may have weakened the catalytic activity. Wang et al. examined the catalytic performance of the C-AuNPs and reported that the presence of citrate decreased the peroxidase-mimicking catalytic activity of the AuNPs [7].

A selectivity test was conducted by replacing H₂O₂ with oxidants, such as potassium ferricyanide (K₃Fe(CN)₆) and dissolved oxygen (DO), respectively. The absorbances of K₃Fe(CN)₆ and DO were too low, almost negligible, indicating the high sensitivity and specificity of B-AuNPs for H₂O₂ detection accordance with previous published result (see Supplemental Information, Fig. S2(a)) [28]. Fig. S2(b) shows the calibration curve of the absorbance at 655 nm, where H₂O₂ detection was linear in the range, 20 μM to 5 mM, indicating that the catalytic performance of B-AuNPs is dependent on the H₂O₂ concentration. According the above result, B-AuNPs were found to be a suitable catalyst for the detection of H₂O₂ with a detection limit of 20 μM.

CONCLUSION

Highly stable negatively charged AuNPs were synthesized within 12 h by *S. oneidensis* biofilm on the anode of an MFC. This simple and ecofriendly method provides chemical capping or stabilizing agent-free AuNPs synthesis as well as in situ decoration on the anode electrode without a binder. The MFC with the AuNPs decorated anode electrode produced 62.5% higher power density (46.37 Wm⁻³) than the plain carbon foam electrode-equipped MFC. The decoration of AuNPs on carbon foam increased the conductivity, decreased the internal resistance, and enhanced biofilm formation on the anode, thereby improving the MFC performance. Moreover, the biogenic as-synthesized AuNPs solution exhibited peroxidase-mimicking activity and allowed the rapid detection of hydrogen peroxide at very low concentrations (20 μM). This MFC-assisted synthesis of AuNPs provides an opportunity for binder-free electrode modification and to produce large scale, chemical-free AuNPs, which can be suitable for sensitive biomedical applications, such as drug delivery, phototherapy cancer detection, and other related fields.

ACKNOWLEDGEMENTS

This study was supported by Priority Research Centers Program (grant no.: 2014R1A6A1031189) through the National Research

Foundation of Korea funded by the Ministry of Education in Korea.

SUPPORTING INFORMATION

Additional information as noted in the text. This information is available via the Internet at <http://www.springer.com/chemistry/journal/11814>.

REFERENCES

1. S. Longo, B. M. d'Antoni, M. Bongards, A. Chaparro, A. Cronrath, F. Fatone, J. M. Lema, M. Mauricio-Iglesias, A. Soares and A. Hospido, *Appl. Energy*, **179**, 1251 (2016).
2. M. E. Khan, M. M. Khan, B.-K. Min and M. H. Cho, *Sci. Rep.*, **8**, 1723 (2018).
3. X. Cao, X. Huang, P. Liang, K. Xiao, Y. Zhou, X. Zhang and B. E. Logan, *Sci. Technol.*, **43**, 7148 (2009).
4. C. Donovan, A. Dewan, H. Peng, D. Heo and H. Beyenal, *J. Power Sources*, **196**, 1171 (2011).
5. M. R. Khan, M. Karim and M. Amin, *Int. J. Eng. Technol.*, **1**, 231 (2012).
6. L. Woodward, M. Perrier, B. Srinivasan, C. Hc and B. Tartakovskiy, *Biotechnol. Prog.*, **25**, 676 (2009).
7. S. Li, C. Cheng, H.-W. Liang, X. Feng and A. Thomas, *Adv. Mater.*, **29**, 1700707 (2017).
8. C. E. Zhao, P. P. Gai, R. B. Song, Y. Chen, J. R. Zhang and J. J. Zhu, *Chem. Soc. Rev.*, **46**, 1545 (2017).
9. W. Guo, Y. Pi, H. Song, W. Tang and J. Sun, *Colloids Surf. A*, **415**, 105 (2012).
10. F. A. a. Alatraktchi, Y. Zhang and I. Angelidaki, *Appl. Energy*, **116**, 216 (2014).
11. S. Her, D. A. Jaffray and C. Alle, *Adv. Drug Deliv. Rev.*, **109**, 84 (2017).
12. M. Christwardana, Y. Chung, D. C. Tannia and Y. Kwon, *Korean J. Chem. Eng.*, **35**(12), 2421 (2018).
13. G. Hartung and G. Mansoori, *J. Nanomater. Mol. Nanotechnol.*, **21**, 17 (2013).
14. A. K. Mittal, Y. Chisti and U. C. Banerjee, *Biotechnol. Adv.*, **31**, 346 (2013).
15. P. S. Vankar and D. Bajpai, *Indian J. Biochem. Biophys.*, **47**, 157 (2010).
16. S. K. Das and E. Marsili, *Rev. Environ. Sci. Biotechnol.*, **9**, 199 (2010).
17. K. D. Z. Duarte, D. Frattini and Y. Kwon, *Appl. Energy*, **256**, 113912 (2019).
18. A. K. Suresh, D. A. Pelletier, W. Wang, M. L. Broich, J.-W. Moon, B. Gu, D. P. Allison, D. C. Joy, T. J. Phelps and M. J. Doktycz, *Acta Biomater.*, **7**, 2148 (2011).
19. V. J. Watson and B. E. Logan, *Biotechnol. Bioeng.*, **105**, 489 (2010).
20. H.-C. Flemming and J. Wingender, *Nat. Rev. Microbiol.*, **8**, 623 (2010).
21. B. A. Nevius, Y. P. Chen, J. L. Ferry and A. W. Decho, *Ecotoxicology*, **21**, 2205 (2012).
22. S. Chen, X. Chen, S. Hou, P. Xiong, Y. Xiong and F. Zhang, *RSC Adv.*, **6**, 114937 (2016).
23. S. Wang, W. Chen, A.-L. Liu, L. Hong, H.-H. Deng and X.-H. Lin, *ChemPhysChem*, **13**, 1199 (2012).
24. O. S. Wolfbeis, A. Dürkop, M. Wu and Z. Lin, *Angew. Chem. Int.*

- Ed.*, **41**, 4495 (2002).
25. S. Guo and S. Dong, *TrAC Trends Anal. Chem.*, **28**, 96 (2009).
26. T. H. Han, S. Y. Sawant, S.-J. Hwang and M. H. Cho, *RSC Adv.*, **6**, 25799 (2016).
27. S. Y. Sawant, T. H. Han, S. A. Ansari, J. H. Shim, A. T. N. Nguyen, J.-J. Shim and M. H. Cho, *J. Ind. Eng. Chem.*, **60**, 431 (2018).
28. M. M. Khan, S. A. Ansari, J. Lee and M. H. Cho, *ACS Sustain. Chem. Eng.*, **2**, 423 (2014).
29. J. Jayapriya, J. Gopal, V. Ramamurthy, U. K. Mudali and B. Raj, *Compos. Part B: Eng.*, **43**(3), 1329 (2012).
30. T. H. Han, J.-H. Lee, M. H. Cho, T. K. Wood and J. Lee, *Res. Microbiol.*, **162**, 108 (2011).
31. Y. Jv, B. Li and R. Cao, *Chem. Commun.*, **46**, 8017 (2010).
32. A. Majzik, R. Patakfalvi, V. Hornok and I. Dékány, *Gold Bull.*, **42**, 113 (2009).
33. M. E. Khan, T. H. Han, M. M. Khan, M. R. Karim and M. H. Cho, *ACS Appl. Nano Mater.*, **1**, 2912 (2018).
34. M. E. Khan, M. M. Khan and M. H. Cho, *RSC Adv.*, **5**, 26897 (2015).
35. S. Kalathil, J. Lee and M. H. Cho, *ChemSusChem*, **6**, 246 (2013).
36. Y. Chen, X. Gu, C.-G. Nie, Z.-Y. Jiang, Z.-X. Xie and C.-J. Lin, *Chem. Commun.*, **33**, 4181 (2005).
37. Z. Zhou, H. Zhang, Y. Zhou, H. Qiao, A. Gurung, R. Naderi, H. Elbohy, A. L. Smirnova, H. Lu, S. Chen and Q. Qiao, *Sci. Rep.*, **7**, 1440 (2017).
38. A. Thill, O. Zeyons, O. Spalla, F. Chauvat, J. Rose, M. Auffan and A. M. Flank, *Environ. Sci. Technol.*, **40**, 6151 (2006).
39. J. L. Ferry, P. Craig, C. Hexel, P. Sisco, R. Frey, P. L. Pennington, M. H. Fulton, I. G. Scott, A. W. Decho, S. Kashiwada, C. J. Murphy and T. J. Shaw, *Nat. Nanotechnol.*, **4**, 441 (2009).
40. S. Y. Sawant, T. H. Han, S. A. Ansari, J. H. Shim, A. T. N. Nguyen, J.-J. Shim and M. H. Cho, *J. Ind. Eng. Chem.*, **60**, 431 (2018).
41. S. G. Mohamed, C.-J. Chen, C. K. Chen, S.-F. Hu and R.-S. Liu, *ACS Appl. Mater. Interfaces*, **6**, 22701 (2014).
42. T. H. Han, D. Mohapatra, N. Mahato, S. Parida, J. H. Shim, A. T. N. Nguyen, V. Q. Nguyen, J.-J. Shim and M. H. Cho, *J. Ind. Eng. Chem.*, **81**, 269 (2020).
43. N. Mahato and M. H. Cho, *Constr. Build. Mater.*, **115**, 618 (2016).
44. R. J. Emerson, T. S. Bergstrom, Y. Liu, E. R. Soto, C. A. Brown, W. G. McGimpsey and T. A. Camesano, *Langmuir*, **22**, 11311 (2006).
45. M. Sun, F. Zhang, Z.-H. Tong, G.-P. Sheng, Y.-Z. Chen, Y. Zhao, Y.-P. Chen, S.-Y. Zhou, G. Liu, Y.-C. Tian and H.-Q. Yu, *Biosens. Bioelectron.*, **26**, 338 (2010).
46. J. C. Biffinger, J. Pietron, O. Bretschger, L. J. Nadeau, G. R. Johnson, C. C. Williams, K. H. Nealson and B. R. Ringeisen, *Biosens. Bioelectron.*, **24**, 900 (2008).
47. F. Gaboriaud, E. Dague, S. Bailet, F. Jorand, J. Duval and F. Thomas, *Colloids Surf. B: Biointerfaces*, **52**, 108 (2006).
48. B. E. Logan, B. Hamelers, R. Rozendal, U. Schröder, J. Keller, S. Freguia, P. Aelterman, W. Verstraete and K. Rabaey, *Environ. Sci. Technol.*, **40**, 5181 (2006).
49. B. E. Logan, *ChemSusChem*, **5**(6), 988 (2012).
50. P. D. Josephy, T. Eling and R. P. Mason, *J. Biol. Chem.*, **257**(7), 3669 (1982).
51. T. H. Han, M. M. Khan, J. Lee and M. H. Cho, *J. Ind. Eng. Chem.*, **20**, 2003 (2014).